scientific reports

Check for updates

OPEN

Magnetostructural coupling in $RFeO_3$ (R = Nd, Tb, Eu and Gd)

R. Vilarinho[1]✉, M. C. Weber[2,3], M. Guennou[4], A. C. Miranda[1], C. Dias[1], P. Tavares[5], J. Kreisel[4], A. Almeida[1] & J. Agostinho Moreira[1]

We investigate the interplay of magnetization and lattice vibrations in rare-earth orthoferrites $RFeO_3$, with a specific focus on non-symmetry-breaking anomalies. To do so, we study the magnetization, magnon excitations and lattice dynamics as a function of temperature in $NdFeO_3$, $TbFeO_3$, $EuFeO_3$ and $GdFeO_3$. The magnetization shows distinct temperature anomalous behavior for all investigated rare-earth orthoferrites, even in the compounds with no phase transitions occurring at those temperatures. Through spin–phonon coupling, these magnetic changes are mirrored by the FeO_6 rotation mode for all the studied $RFeO_3$, revealing a common magnetostructural effect associated with the octahedra rotations. The R^{3+} oscillation modes evidence a Fe^{3+}/R^{3+} spins cross-talk for the $NdFeO_3$ and $TbFeO_3$ cases. Our work sheds light into the common magnetostructural coupling in rare-earth orthoferrites, and the important role of magnetic anisotropy and spin–orbit coupling strength of the R–Fe interactions on the spin-reorientation transition at high temperatures.

Rare-earth orthoferrites $RFeO_3$ (R = rare-earth trivalent cation), despite being studied for decades[1–6], attracted recent scientific interest thanks to their intriguing magnetic properties, including spin-reorientation transitions and new-found magnetically induced ferroelectricity[7–12].

The Fe^{3+} spins order at T_N between 623 and 740 K, with increasing temperature for increasing rare-earth cation size[5,13]. The ordering is triggered by the condensation of the magnetic order parameter with symmetry $m\Gamma_4^+$. This gives rise to an $A_xF_yG_z$-type ordering of the Fe^{3+} spin sublattice (in Bertaut notation)[14] with the magnetic space group P$n'ma'$. The primary magnetic order is of the antiferromagnetic G-type. The canted spin structure leads to a net-magnetization along the b-axis[5,13]. The R^{3+} spin-sublattice orders below 10 K. Like the Fe^{3+} spin-sublattice, a G-type order dominates the magnetic structure of the R^{3+} spin-sublattice. The interaction of both G-type lattices can give rise to improper ferroelectricity, as for instance in $GdFeO_3$ below 3 K[9,12,15,16].

Between T_N and the temperature of R^{3+} spin ordering, the magnetic landscape is dominated by the crosstalk of the ordered iron sublattice and the paramagnetic rare-earth spins. On the one hand, rare-earth ions with a significant magnetocrystalline anisotropy trigger a spin reorientation transition of the magnetic iron sublattice (e.g. R = Nd, Sm, Er and Tb)[5]. On the other hand, the iron sublattice induces a net magnetization of the rare-earth sublattice. It was suggested that parallel or antiparallel alignment of the R^{3+} spin sublattice with respect to the Fe^{3+} one is steered by the octahedron tilt system, thus linking the crystal structure and magnetism[17].

In this intermediate regime, temperature-dependent magnetic anomalies were reported. For instance, the M(T) curves of $GdFeO_3$ and $TbFeO_3$ exhibit s-like anomalies at around 210 and 250 K, respectively[1,6]. However, their origins and link to the crystal structure and lattice vibrations remain still unclear.

Our present work is motivated by the need to shed light on these aspects aiming for a deeper understanding of the magnetic behavior in $RFeO_3$. Towards this objective, we scrutinize the magnetization, and Raman-active magnons and phonons across a large temperature range of a series of $RFeO_3$: $NdFeO_3$, $TbFeO_3$, $EuFeO_3$ and $GdFeO_3$. We selected these four compounds for their different rare-earth magnetic properties and interplay between magnetic and lattice degrees of freedom, to allow the access to different magnetic interactions between the Fe^{3+} and the R^{3+} spins. For instance, both $NdFeO_3$ and $TbFeO_3$ exhibit spin-reorientation transitions, yet at different temperatures, and hence a significant magnetocrystalline anisotropy. On the other hand, Gd^{3+} ions present no magnetocrystalline anisotropy of spin–orbit origin (i.e. zero orbital moment, with a large spin moment) and Eu^{3+} has no magnetic moment. Therefore, this set of compounds is representative for the family of orthoferrites in general. From the comprehensive study of the temperature dependence of the magnetization and

[1]IFIMUP, Departamento de Física e Astronomia, Faculdade de Ciências, Universidade do Porto, rua do Campo Alegre s/n, 4169-007 Porto, Portugal. [2]Department of Materials, ETH Zurich, Vladimir-Prelog-Weg 4, 8093 Zurich, Switzerland. [3]Institut des Molécules et Matériaux du Mans, UMR 6283 CNRS, Le Mans Université, 72085 Le Mans, France. [4]Department of Physics and Materials Science, University of Luxembourg, 41 Rue du Brill, 4422 Belvaux, Luxembourg. [5]Centro de Química, Departamento de Química, Universidade de Trás-os-Montes e Alto Douro, 5000-801 Vila Real, Portugal. ✉email: rvsilva@fc.up.pt

magnon wavenumbers, different types of magnetic anomalies are ascertained, which are not associated with non-symmetry-breaking. These magnetic changes are mirrored in the FeO_6-rotation and R-oscillation modes, via spin–phonon coupling. Our experimental results show a common magnetostructural effect occurring in these $RFeO_3$ associated with the FeO_6 octahedra rotations, and a cross-talking between Fe^{3+} spins and the R^{3+} spins for the $NdFeO_3$ and $TbFeO_3$ cases that exposes the importance of magnetic anisotropy and spin–orbit coupling in triggering the spin-reorientation transition.

Methods

High-quality ceramic pellets of $RFeO_3$ (R = Nd, Eu, Gd and Tb) were processed through the urea sol–gel combustion method, sintered at 1350 °C for 60 h, quenched to room temperature. X-ray powder diffraction patterns were recorded at ambient conditions using an X'Pert Pro PANalytical diffractometer with a copper anode (1.54184 Å) in Bragg–Brentano geometry and an ultrafast X'Celerator detector with a secondary monochromator, from 10° to 95° in 2θ. Rietveld refinements of the diffraction patterns confirm the correct *Pnma* space group (see Fig. S1 of Supplemental Material). No secondary phases were detected, except in $NdFeO_3$ ceramics, which show an amount of 6.8% of Nd_2O_3.

Low-field DC induced specific magnetization measurements were carried out using commercial superconducting quantum interference SQUID magnetometer. The magnetization was measured after zero-field (ZFC) and field cooling (FC) from 5 to 380 K under an applied magnetic field of 40 Oe, with a resolution of 1×10^{-7} emu.

Raman spectra were recorded using a Jobin–Yvon T64000 spectrometer and a Renishaw inVia Qontor with 514.5 nm and 532 nm linearly polarized excitation lines of Ar^+ and diode-pumped lasers, respectively. The spectral ranges cover 100 to 800 cm^{-1} and − 600 to 600 cm^{-1}. Measurements were performed at fixed temperatures from 10 to 875 K using either a closed-cycle helium cryostat or a THMS600 Linkam Stage. The effect of the laser power on the sample was previously studied and it was limited below 5 mW to prevent sample heating. The best fits of a sum of damped oscillators to the measured Raman spectra allow us to determine the wavenumbers of the phonon and magnon modes[18].

Experimental result s and discussion

Magnetic properties and interactions. In the first step of our study, we investigate the temperature dependence of the magnetization for $NdFeO_3$ (FC), $TbFeO_3$, $EuFeO_3$ and $GdFeO_3$ (ZFC), as displayed in Fig. 1. The vertical dashed arrows mark the temperatures of anomalies that will be important for the following sections of this work. Remarkably, the magnetization curves have little in common and the magnetization signals are dramatically different for different rare-earths. This motivates the following detailed analysis.

$NdFeO_3$. The magnetization of $NdFeO_3$ (Fig. 1a) is temperature independent between 350 and 175 K. With the start of the spin reorientation from $A_xF_yG_z$ (*Pn'ma'*) to $C_xG_yF_z$-type order (*Pn'm'a*) at 170 K, M(T) increases monotonously until a small dent at 110 K marks the end of the spin reorientation regime[19]. Down to 70 K, M(T) further increases. Hereafter, the magnetization decreases due to the gradual antiparallel ordering of the Nd^{3+} spins in the exchange field of the Fe^{3+} spins[7]. At 9 K, the magnetic contributions of the Nd^{3+} and Fe^{3+} spins compensate and the magnetization reverses for lower temperatures. The M(T) profile of the ceramic sample qualitatively agrees with the vector sum of the *b*-axis and *c*-axis components of the magnetization for single crystal measurements taken from Ref.[7] (see inset of Fig. 1a).

$TbFeO_3$. In Fig. 1b, M(T) of $TbFeO_3$ increases with decreasing temperature with changes in slope for several temperature intervals. At 280 K and at 150 K, the slope of M(T) increases slightly (see Fig. S2 of Supplemental Material for a detailed view). These features were reported earlier, however, remain to be understood[6]. Below 20 K, the slope of M(T) becomes steeper with a maximum at 10 K. The sudden increase in slope at 20 K marks the onset of the spin-reorientation transition, where the net magnetic moment of the Fe^{3+} spins rotates from the *b*- to the *c*-axis. In addition, the Tb^{3+} spins order in the exchange field of the Fe^{3+} spins below 10 K, reflected by the saturation of M(T) in good agreement with the literature[10–20].

$EuFeO_3$ and $GdFeO_3$ do not show a spin-reorientation transition[13]. Nevertheless, the M(T) curve of both materials is characterized by anomalies with clear changes in slope. The magnetization of $EuFeO_3$ increases as the temperature decreases toward its maximum at 30 K, presenting a broad anomaly around 200 K. Also a broad maximum of M(T) around 200 K was reported in the literature for $EuFeO_3$, with the magnetization decreasing towards 0 K[21]. The temperature dependence of the magnetization of $GdFeO_3$ is more complex, exhibiting strong variations below 100 K. For T < 36 K, the magnetization increases due to the paramagnetic response of the Gd^{3+} sublattice[22]. Qualitatively, the M(T) curve of $GdFeO_3$ agrees with the results reported in the literature[1,21]. The existence of magnetic changes occurring at 260 K is also ascertained by the anomalous temperature dependence of the coercive field at 200 K[23].

Among the four studied compounds and in the 5 to 350 K range, $TbFeO_3$ presents the highest maximum magnetization value (around 500 emu/mol), while $EuFeO_3$ presents the smallest one (around 0.5 emu/mol, 3 orders of magnitude smaller than $TbFeO_3$). $GdFeO_3$ and $NdFeO_3$ are in between, with $GdFeO_3$ presenting a larger magnetization below 150 K. Due to the van Vleck character of Eu^{3+}, its spins are expected to contribute little to the total magnetization contrary to the other rare-earth cations[24]. Thus, the magnetization of $EuFeO_3$ arises dominantly from the Fe^{3+} spin sublattice, due to the canting of the Fe^{3+} spins, which is found in literature to be 8.0 mrad[4]. Despite the similar canting angles of $NdFeO_3$, $GdFeO_3$ and $TbFeO_3$, these compounds show a substantially larger magnetization than $EuFeO_3$[4]. Therefore, we conclude that the contribution of the Nd^{3+}, Gd^{3+}, and Tb^{3+} paramagnetic momenta or their interaction with Fe^{3+} add a significant contribution for the overall magnetization. In the case of $TbFeO_3$ and $GdFeO_3$, the R^{3+} spins align parallelly to the net magnetization of the Fe^{3+} spins, leading to an increase of the overall magnetization. The Nd^{3+} spins, in turn, align antiparallelly to the Fe^{3+} spins. Hence, the magnetization decreases and even reverses at low temperatures.

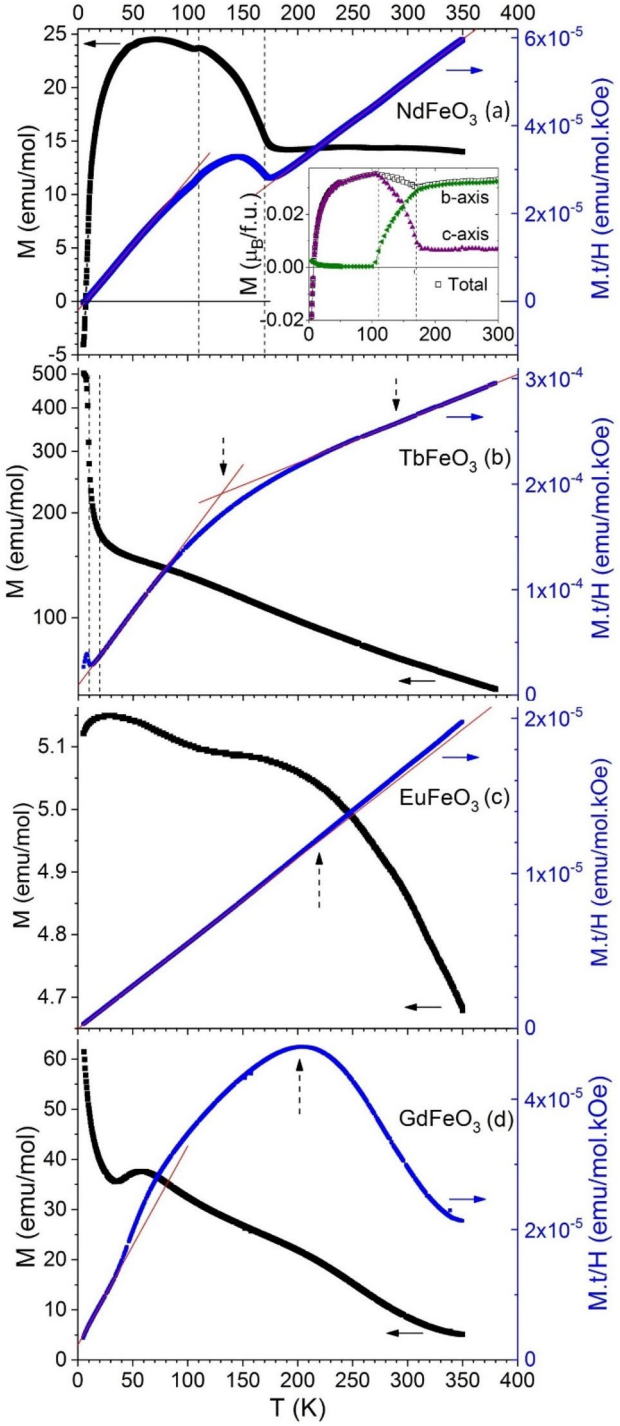

Figure 1. Left axes: temperature dependence of the magnetization of (**a**) $NdFeO_3$ under FC conditions, and (**b**) $TbFeO_3$, (**c**) $EuFeO_3$ and (**d**) $GdFeO_3$, under ZFC conditions, measured in heating under 40 Oe. Inset of (**a**) shows similar M(T) data for a $NdFeO_3$ single crystal from Ref.[7]. Right axes: M.t/H ($t = T/T_N$) versus temperature for the same compounds. Vertical dashed lines mark the phase transition temperatures following Ref.[13], while vertical dashed arrows mark relevant anomalies.

Figure 2 summarizes the temperatures where discernable magnetic anomalies are observed for each $RFeO_3$. Apart from the spin-reorientations of $NdFeO_3$ and $TbFeO_3$, these anomalies below T_N do not correspond to any critical phenomena or phase transitions. The observed anomalies in the M(T) curves, which are between 3 and 4 orders of magnitude larger than the measurement resolution, indicate complex magnetic interactions in the investigated orthoferrites, triggered by the interaction between Fe^{3+} and R^{3+} spins, which we analyze in the following.

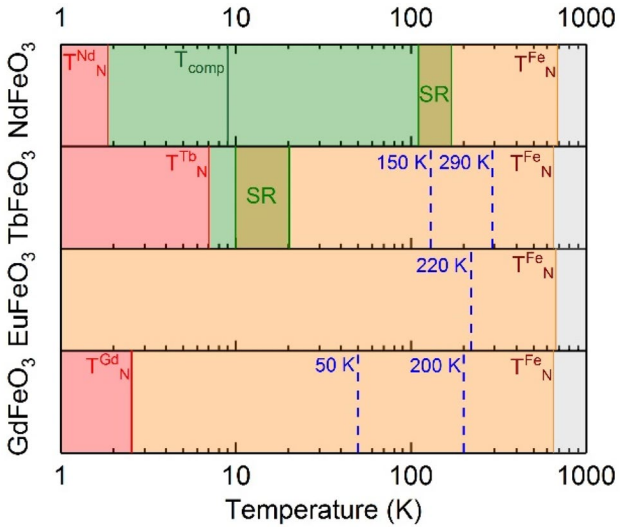

Figure 2. Magnetic phase sequence for RFeO$_3$ with R = Nd, Tb, Eu and Gd. Critical temperatures of the reported phase transitions taken from Refs.[10,13,25]. Dashed lines mark relevant anomalies observed in this work on M(T) curves, not associated with phase transitions.

Compound	$\langle d \rangle \times 10^3$	ΔT_{fit} (K)
$NdFeO_3$	− 10.24 ± 0.03	11–52
$TbFeO_3$	10.3 ± 0.1	18–70
$EuFeO_3$	− 0.62 ± 0.05	5–160
$GdFeO_3$	11.3 ± 0.1	13–34

Table 1. Mean R–Fe interaction parameter $\langle d \rangle$ calculated from the best fit of Eq. (1) to the experimental data shown in Fig. 1a–d, and the temperature interval where the fit is performed.

In the molecular field approximation, we can express the net magnetization resulting from the interaction of the order Fe^{3+} sublattice and the paramagnetic R^{3+} spins as follows[2]:

$$M(T) = 2\alpha\sigma(T)\left[1 + \frac{\langle d \rangle}{t}\right], \tag{1}$$

where α is the spin canting angle, σ(T) the Fe^{3+} sublattice moment, $\langle d \rangle$ the mean R–Fe interaction parameter and $t = T/T_N$. The plot of $F(t) = M(T)t/H$ versus T is represented by the blue curves (right axes) of Fig. 1. Here, $H \propto \sigma(T)/\sigma(0)$ is the effective magnetic field, calculated from Mössbauer data[4], and $\sigma(0)$ is the Fe^{3+} sublattice magnetic moment at 0 K. According to the molecular field approximation, the changes of the slope of $F(t)$, thus of $2\alpha\sigma(0)/T_N$, evidence changes of net magnetization of the iron sublattice[2]. From the intercept with $t = 0$, we calculate $\langle d \rangle$ associated with the magnetic interaction strength between R^{3+} and Fe^{3+} spins[2].

$NdFeO_3$ presents two linear regimes above and below the spin reorientation transition. The slope in the 10 to 60 K range is about 59% steeper than above the spin reorientation. We interpret this as a consequence of the emergent magnetic interaction of Nd^{3+} and Fe^{3+} spins below the spin reorientation regime.

$TbFeO_3$ also exhibits two linear regimes in the 20 to 80 K and 250 to 350 K in $F(t)$, respectively, with a slope decrease of about 70% as temperature increases, in agreement with the literature[20]. The deviation below 260 K from the high temperature linear regime can be better observed in the residuals plot obtained from subtraction of the linear fit to the data, shown Fig. S2 of the Supplemental Material.

$EuFeO_3$ exhibits two different linear temperature dependences from 5 to 150 K, and 230 to 350 K, respectively, with only a minor slope change, of the order of 4%. This is in agreement with small variation of magnetization with temperature[20].

$GdFeO_3$, displays the most complex $F(t)$ behavior, with linear relations from 10 to 35 K, 100 to 150 K and 250 to 300 K and a local maximum at 200 K. Such a behavior suggests that the model does not fully reproduce the magnetic properties of $GdFeO_3$ above 150 K, but this shall not invalidate the calculation of the $\langle d \rangle$ value at very low temperatures.

The calculated $\langle d \rangle$ values are presented in Table 1. For the fitting, the linear regime at low temperatures (see Table 1) was used, where the R–Fe magnetic interaction is strongest. The $\langle d \rangle$ values are about one order of magnitude smaller than those reported by Treves[2], which were calculated from data available only above 100 K. For comparison with Treves, we have analyzed our data in the same temperature range, then leading to similar

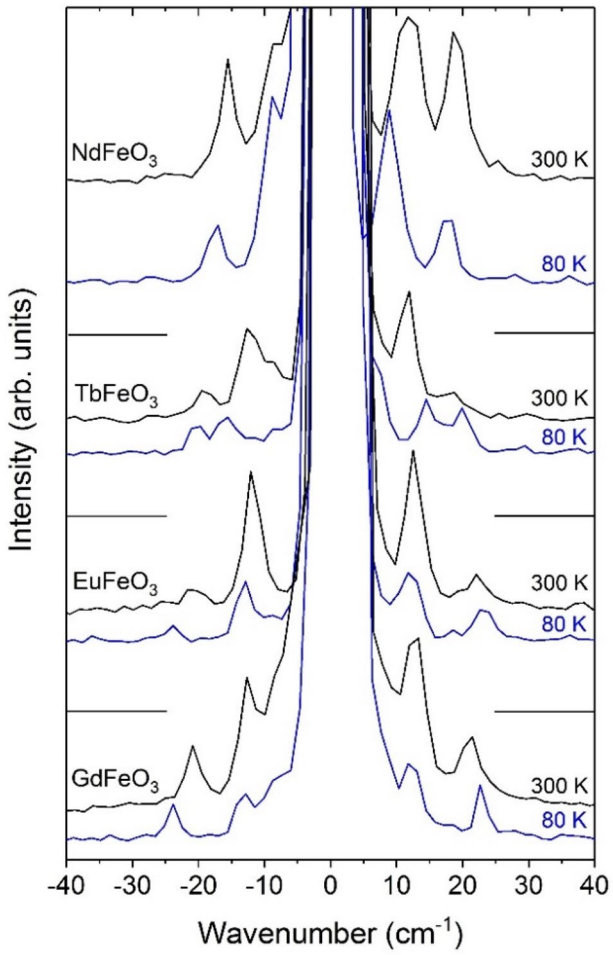

Figure 3. Representative unpolarized Stokes and anti-Stokes Raman spectra of $RFeO_3$ (R = Nd, Eu, Gd and Tb), in the −40 to 40 cm^{-1} spectral range, recorded at 80 and 300 K.

values. The difference is thus due to the analyzed temperature regime, and we consider that our fittings to the lower temperature range more correctly account the underlying physics.

For $NdFeO_3$, $\langle d \rangle$ is negative. This indicates antiferromagnetic interaction between Nd^{3+} and Fe^{3+} spins, in good agreement with the Nd^{3+} spin ordering antiparallel to the Fe^{3+} spins. For $GdFeO_3$ and $TbFeO_3$, $\langle d \rangle$ is positive. This leads to a parallel alignment of Tb^{3+}/Gd^{3+} and Fe^{3+} spins and explains the increase in overall magnetization and the absence of a compensation temperature. We note, that these values are in agreement with the theoretical ones for the orientation of the rare-earth sublattice magnetization with respect to the Fe^{3+} spins sublattice[17]. Among the studied compounds, the mean interaction coupling parameter between Eu^{3+} and Fe^{3+} cations has the smallest absolute value. This indicates a comparably small interaction between both ions and can be understood by the small magnetic momentum of the Eu^{3+} cations.

It is worth to stress that, although the values of $\langle d \rangle$ are similar for both $GdFeO_3$ and $TbFeO_3$, the anisotropy of $TbFeO_3$ is larger, such that $TbFeO_3$ shows a spin-reorientation transition whereas $GdFeO_3$ does not. $NdFeO_3$ and $TbFeO_3$ show a similar R–Fe interaction parameter $\langle d \rangle$, yet of different sign. Also, the spin reorientation temperatures differ significantly for both materials. These behaviors underline the complexity of magnetic interactions in rare-earth orthoferrites.

Magnon excitations. We now investigate the magnetic changes through a temperature-dependent analysis of collective spin excitations of the Fe^{3+} spin lattice, so-called magnons. Magnons are known to be an excellent probe of subtle magnetic changes, such as the beforehand reported anomalies in $RFeO_3$ with R = Y, Sm, Dy, Ho, Tm, Er and Tb[5,26–28].

Figure 3 shows the unpolarized Stokes and anti-Stokes Raman spectra of $NdFeO_3$, $TbFeO_3$, $EuFeO_3$ and $GdFeO_3$ recorded at 80 and 300 K. Two magnon modes are observed, in good agreement with earlier experiments on other $RFeO_3$[26,27,29]. According to literature, the lower wavenumber mode (M1) is assigned to the ferromagnetic magnon and the higher wavenumber mode (M2) to the antiferromagnetic magnon of the Fe^{3+} spin-sublattice[26,27].

Figure 4a–h show the temperature dependence of the wavenumber of the M1 and M2 magnons of $NdFeO_3$, $TbFeO_3$, $EuFeO_3$ and $GdFeO_3$, respectively, from 80 to 450 K. For completion, we also show in Fig. 4b,f the

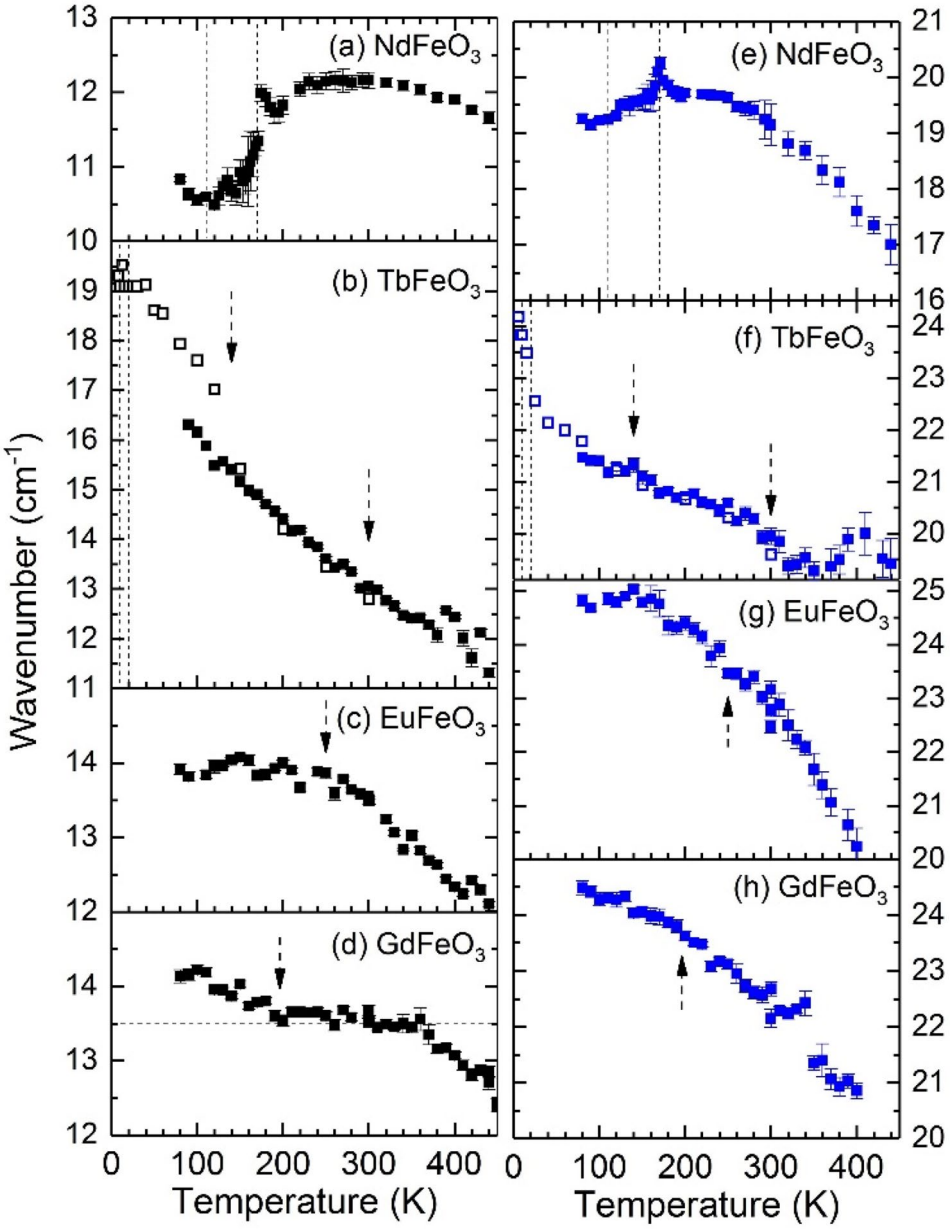

Figure 4. Temperature dependence of the wavenumber of the magnons M1 (left) and M2 (right) observed in $NdFeO_3$, $TbFeO_3$, $EuFeO_3$ and $GdFeO_3$. Open symbols for $TbFeO_3$ were taken from Ref.[27]. Vertical dashed lines mark the spin reorientation temperatures following Ref.[13], while dashed arrows mark relevant M(T) anomalies observed in Fig. 1a–d.

available data from the literature between 6 and 300 K for $TbFeO_3$. We begin by discussing $NdFeO_3$, shown in Fig. 4a,e, which shows a particularly interesting behavior with several regimes. Between 500 and 240 K, the wavenumber of the magnon M1 increases monotonously with decreasing temperature. From 240 to 100 K, the magnon M1 softens by 1.5 cm^{-1}. In addition, cusp-like anomalies mark the limits of the spin-reorientation temperature range (170–110 K). Below 100 K, the wavenumber of magnon M1 increases upon further cooling. Following the interpretation given for $TbFeO_3$ and $SmFeO_3$[26,27], this result is associated with the alignment of the Nd^{3+} spins in the exchange field of the Fe^{3+} spin sublattice. Qualitatively, our temperature dependence of M1 wavenumber for $NdFeO_3$ is in good agreement with the one observed through THz spectroscopy data[30,31]. Magnon M2 hardens on cooling down to 240 K. At the high temperature limit of the spin-reorientation a cusp-like anomaly occurs and, on further cooling down to 78 K, magnon M2 slightly softens.

The temperature dependence of the M1 and M2 magnons wavenumber of $TbFeO_3$ here reported (Fig. 4b,f closed symbols) are in good agreement with the already reported data (open symbols), with only the exception of the points between 80 and 100 K, for the case of M1[27]. The wavenumber of both magnons increases monotonously as the temperature decreases. A clear change of slope of the temperature dependence of M1 is observed

at around 150 K, in the temperature interval for which the change of slope of the $F(t)$ function is observed (cf. Fig. 1b). The wavenumber of the magnon M2 experiences a sudden increase below 20 K, associated with the spin reorientation transition.

The wavenumber of both magnons of $EuFeO_3$, shown in Fig. 4c,g, increases as temperature decreases and no clear anomalous temperature dependence is found down to 80 K. The temperature dependence of the magnon wavenumbers of $GdFeO_3$ are depicted in Fig. 4d,h. The wavenumber of the magnon M2 increases monotonously as temperature decreases towards 80 K, without any hint of anomalous behavior. However, the wavenumber of M1 increases as temperature decreases from 450 K down to 350 K, then it becomes temperature independent down to 200 K, and on further cooling, the wavenumber of magnon M1 increases linearly down to 100 K.

Among the studied compounds, the magnon wavenumbers of $TbFeO_3$ exhibit the largest temperature variation, reaching more than 6 cm^{-1} for M1, while the smallest variations are found in $EuFeO_3$ and are less than 1 cm^{-1} for M1 and 4 cm^{-1} for the M2 mode, in agreement with their respective largest and smallest magnetization changes (cf. Fig. 1). We can conclude that the anomalies identified in the magnetization curves appear to affect only the M1 mode (seen in $TbFeO_3$ and $GdFeO_3$), while they apparently do not affect the M2 mode, which only presents anomalies at the spin-reorientations (seen in $NdFeO_3$ and $TbFeO_3$). Having in mind the ferromagnetic origin of the M1 magnons, this result points out that the observed magnetic anomalies in $TbFeO_3$ and $GdFeO_3$ might be associated with changes of the ferromagnetic interactions.

Comparing the temperature behavior of the magnons wavenumber in $NdFeO_3$ to other compounds with spin-reorientation, we conclude that M1 exhibits a similar incomplete softening to those reported for $ErFeO_3$, $TmFeO_3$ and $SmFeO_3$, which has been attributed to the coupling between the Fe^{3+} spins and the R^{3+} electronic states[30–33]. In this regard, it seems that M1 has a common temperature dependence for all $RFeO_3$ with spin-reorientation. In contrast, the published results do not exhibit the softening of M2 neither any anomalies seen at the spin-reorientation limits in both magnons wavenumber[26,27], which deserves further more detailed studies of spin excitations across the spin-reorientations of these compounds.

Spin–phonon coupling. In the next step, we investigate the response of the phonon spectra as a function of temperature. The optical phonons of the $RFeO_3$ have A_g, B_{1g}, B_{2g} and B_{3g} symmetries—the mode assignment is available in the literature[34]. Figures 5a–d show unpolarized Raman spectra in the range from 100 to 580 cm^{-1}, for $NdFeO_3$, $TbFeO_3$, $EuFeO_3$ and $GdFeO_3$, respectively, measured at fixed temperatures between 10 and 800 K. The room-temperature Raman signature agrees with literature data[34]. With decreasing temperature, the phonon bands sharpen and shift at different rates. As a consequence, some bands become better resolved and visible.

From the study of the temperature evolution of each observed mode, we chose to present and discuss in more detail two modes, which present the most relevant spin–phonon coupling: the $[010]_{pc}$ in-phase FeO_6 octahedra rotation mode (Fig. 6a–d), and of the out-of-phase R-oscillations modes along the x- and z-axes (Fig. 7a–d). As the magnetic super-exchanges in the Fe^{3+} spin sublattice is tightly associated with the Fe–O–Fe bond angle, the FeO_6 rotation modes are highly sensitive to magnetic changes of the Fe^{3+} spin sublattice. Moreover, since the R-oscillation modes are sensitive to the environment around the R^{3+} cations, we use them as probes of the interaction R–Fe spins interaction. To study the spin–phonon coupling, the phonon wavenumber is compared to the expected anharmonic temperature behavior, obtained from the best fit to the experimental data, above 200 K (for $NdFeO_3$ and $GdFeO_3$) and 300 K (for $TbFeO_3$ and $EuFeO_3$), of the equation[35]

$$\omega(T) = \omega_0 - C\left(1 + \frac{2}{e^{\hbar\omega_0/2k_BT} - 1}\right) - D\left(1 + \frac{3}{e^{\hbar\omega_0/3k_BT} - 1} + \frac{3}{(e^{\hbar\omega_0/2k_BT} - 1)^2}\right), \quad (2)$$

where ω_0, C and D are fitting parameters and k_B is the Boltzmann constant. These fits are given as solid lines in Figs. 6 and 7. It is at first sight surprising that no anomalous temperature dependence is observed at T_N (see Fig. S3 of Supplemental Material), also not found for $YFeO_3$[36].

In the $[010]_{pc}$ in-phase FeO_6 octahedra rotation mode, the spin-reorientation for $NdFeO_3$ reveals itself through anomalies in the temperature dependence of this mode observed in Fig. 6a. Its temperature dependence presents a deviation to higher wavenumbers below 170 K. From 150 to 30 K, the wavenumber linearly increases with decreasing temperature. No anomalous temperature dependence at the low temperature limit of the spin-reorientation transition is observed. Below 20 K, a sudden increase of the wavenumber is observed on approaching the compensation temperature of $NdFeO_3$ at 8 K. In $TbFeO_3$ (Fig. 6b), a strong deviation to higher wavenumbers of the octahedra rotation mode occurs below 300 K. In the case of $EuFeO_3$ (Fig. 6c), a downshift takes place below 250 K, while for $GdFeO_3$ (Fig. 6d), an upshift is observed below 200 K.

For all the studied compounds, the anomalous temperature dependence of the $[010]_{pc}$ in-phase FeO_6 octahedra rotation mode wavenumber is observed at the same temperature where the corresponding M(T) curves exhibit anomalies (marked by the dashed lines and arrows in Fig. 6a–d). This implies the specific role of this mode in the spin–phonon coupling of the studied compounds, even at the spin-reorientation of $NdFeO_3$. The shifts ranging from 1 to 3 cm^{-1}, with the expected magnitude for spin–phonon coupling effects[37–40], would correspond to octahedra rotation changes, estimated to be between 0.05° and 0.15°, arising from the magnetostructural coupling. The Raman mode wavenumber shift are positive, except for $EuFeO_3$. This is associated with the overall different magnetization response of $EuFeO_3$ in comparison to the other compounds as shown in Fig. 1, due to the lack of R–Fe interactions, which leads to a different spin–phonon interaction. This assumption is actually corroborated by the substantially smaller magnitude of the mean interaction parameter $\langle d \rangle$ of Eu–Fe sublattices relatively to the remaining compounds, as it can be straight confirmed from Table 1.

We now aim at understanding the cross-talk of the magnetic R–Fe interaction with the phonon lattice, as recently observed in $SmFeO_3$[40]. To do so, we address the out-of-phase R-oscillations modes, shown in Fig. 7a–d. In general, three different temperature behaviors of these modes are observed.

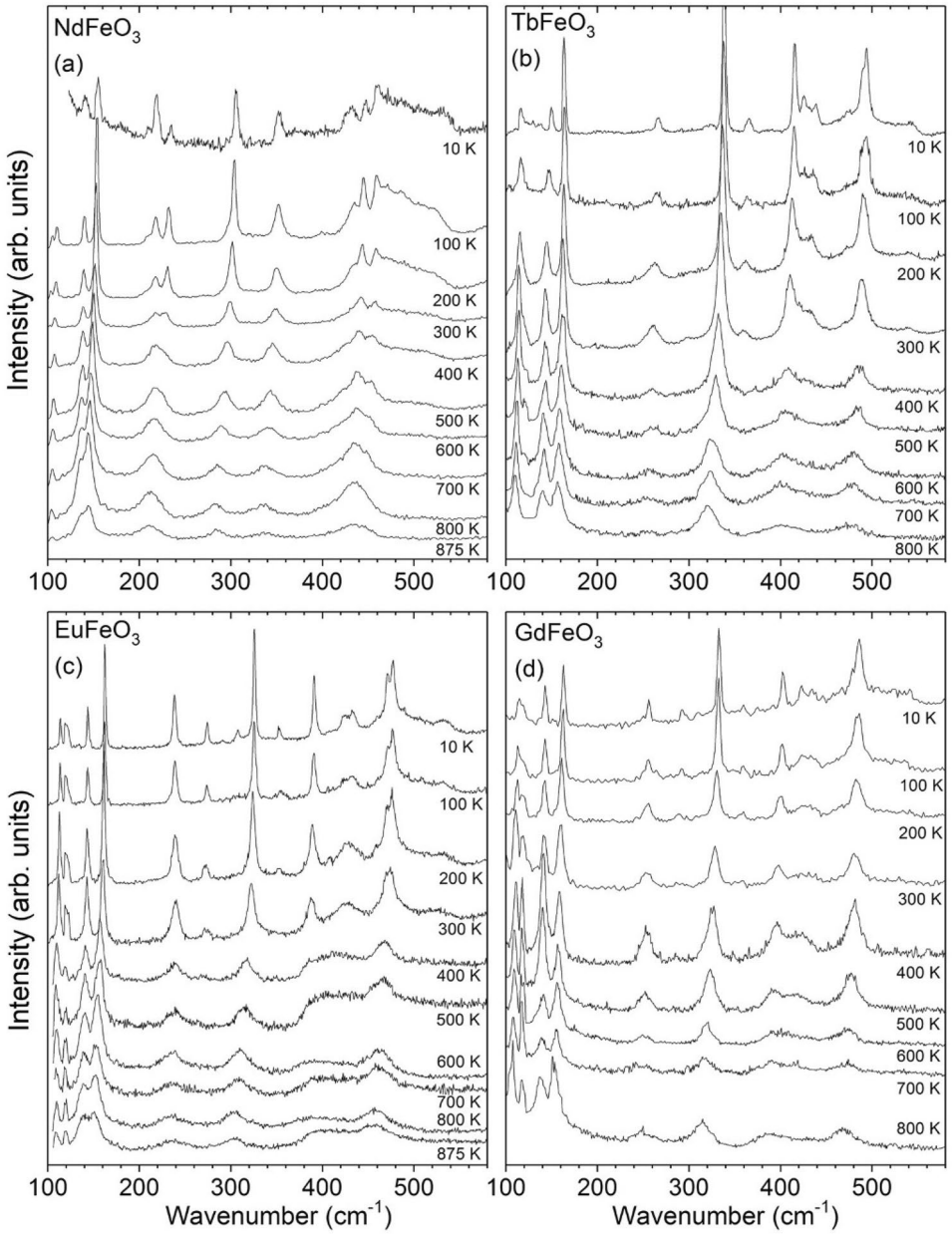

Figure 5. Representative unpolarized Raman spectra of (**a**) $NdFeO_3$, (**b**) $TbFeO_3$, (**c**) $EuFeO_3$ and (**d**) $GdFeO_3$, recorded at different fixed temperatures.

Concerning the two Nd-oscillation modes (Fig. 7a), their wavenumbers follow the anharmonic temperature law down to 110 K, below which a small downshift occurs. On further cooling, they both increases linearly, with a maximum downshift of around 0.5 cm^{-1} at 10 K. Although small, this points out for a coupling between the spin structure and the phonons involving the Nd^{3+} cations.

Figure 7b shows the temperature dependence of the wavenumber of the two Tb-oscillation modes. Below 280 K/150 K, the wavenumber of the Tb(z)/Tb(x) oscillation mode shows a notable upshift/downshift, with a maximum magnitude of 4 cm^{-1}. Each mode starts its deviation at a temperature wherein an anomaly was found in the M(T) curve, evidencing the interaction of the ordered Fe^{3+} spins with the paramagnetic Tb^{3+} spins. Moreover, the different temperature of deviation and direction of the Tb-oscillation modes wavenumber along each crystallographic axis are evidence of a strong magnetic anisotropy which affects the elastic interactions involving the Tb^{3+} cations.

Finally, for $EuFeO_3$ and $GdFeO_3$, the wavenumber of both R(z) and R(x)-oscillation modes follow the expected anharmonic temperature dependence in the investigated range, as shown in Fig. 7c,d, respectively. The absence of a coupling between spins and the R-oscillation modes can be understood by the properties of the Eu^{3+} and Gd^{3+} cations. The van Vleck character of Eu^{3+} cation leads to a small magnitude of the mean interaction parameter $\langle d \rangle$ regarding the magnetic Eu^{3+}–Fe^{3+} interactions[24], which are therefore small. On other hand, Gd^{3+} does not

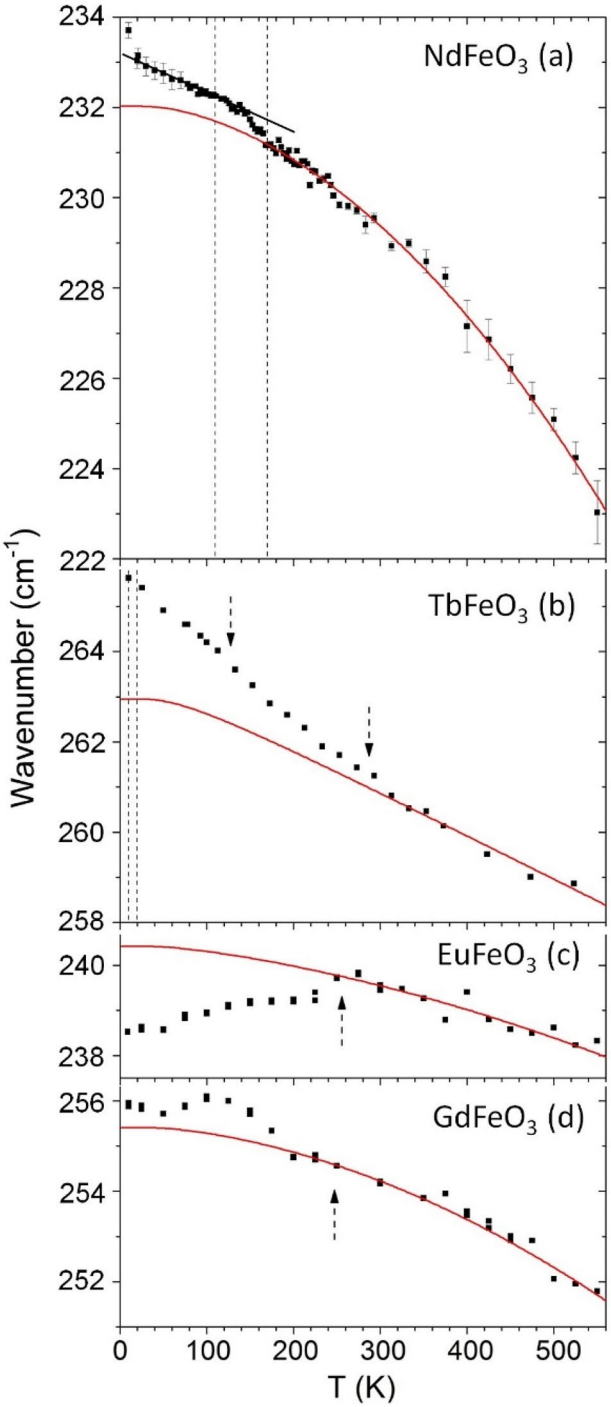

Figure 6. Temperature dependence of the $[010]_{pc}$ in-phase octahedra wavenumber for $NdFeO_3$, $TbFeO_3$, $EuFeO_3$ and $GdFeO_3$. The solid curves were determined by the best fits of the anharmonic temperature law above 200 K (for $NdFeO_3$ and $GdFeO_3$) and 300 K (for $TbFeO_3$ and $EuFeO_3$) and its extrapolation down to 0 K[35]. Vertical dashed lines mark the phase transition temperatures following Ref.[13], while dashed arrows mark relevant M(T) anomalies.

exhibit magnetocrystalline anisotropy and, as it has no orbital angular momentum, the spin–orbit interaction is negligibly small. Consequently, a negligible coupling between Gd^{3+} spin orientation changes and cationic oscillations are expected.

To get further information regarding the coupling between phonons and spins, we investigate the quantitative correlation between the measured magnetization and the contribution $\Delta\omega = \omega_{ph}(T) - \omega_{ph\text{-}anhar}(T)$ to the phonon wavenumber due to changes in the spin structure.

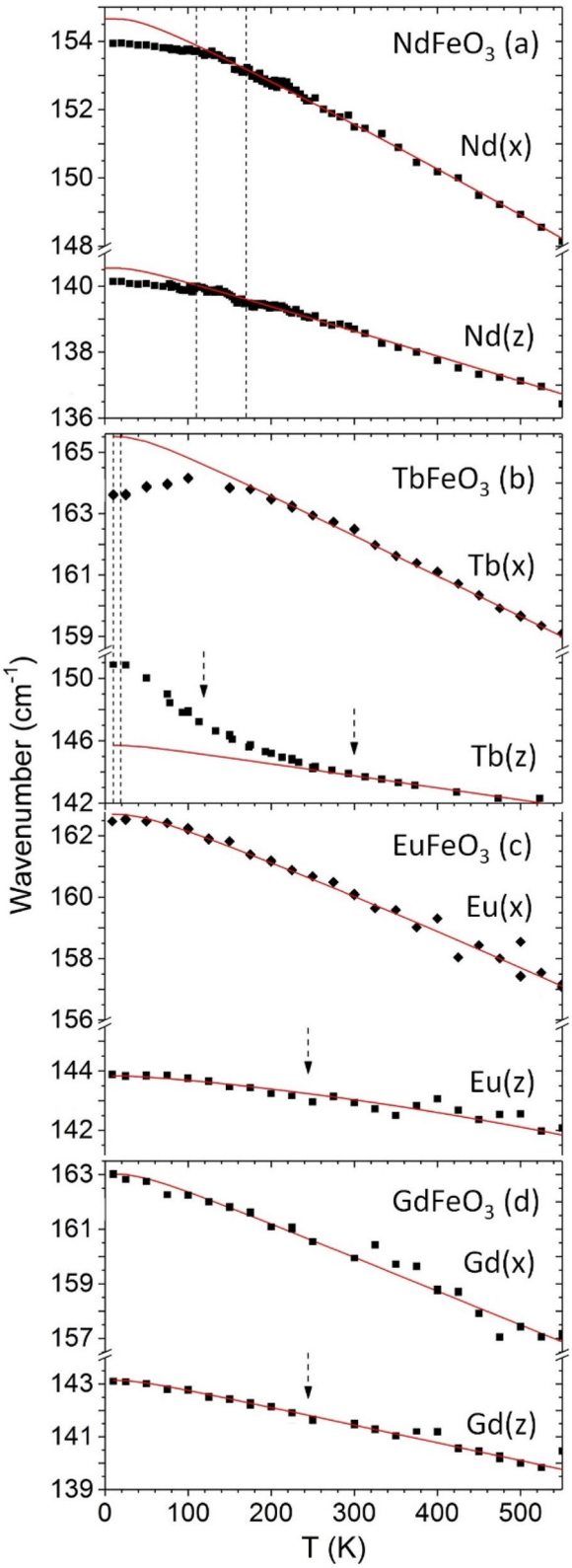

Figure 7. Temperature dependence of the out-of-phase R(x) and R(z)-oscillations wavenumber for $NdFeO_3$, $TbFeO_3$, $EuFeO_3$ and $GdFeO_3$. The solid curves were determined by the best fits of the anharmonic temperature law above 200 K (for $NdFeO_3$ and $GdFeO_3$) and 300 K (for $TbFeO_3$ and $EuFeO_3$) and its extrapolation down to 0 K[35]. Vertical dashed lines mark the phase transition temperatures following Ref.[13], while dashed arrows mark relevant M(T) anomalies.

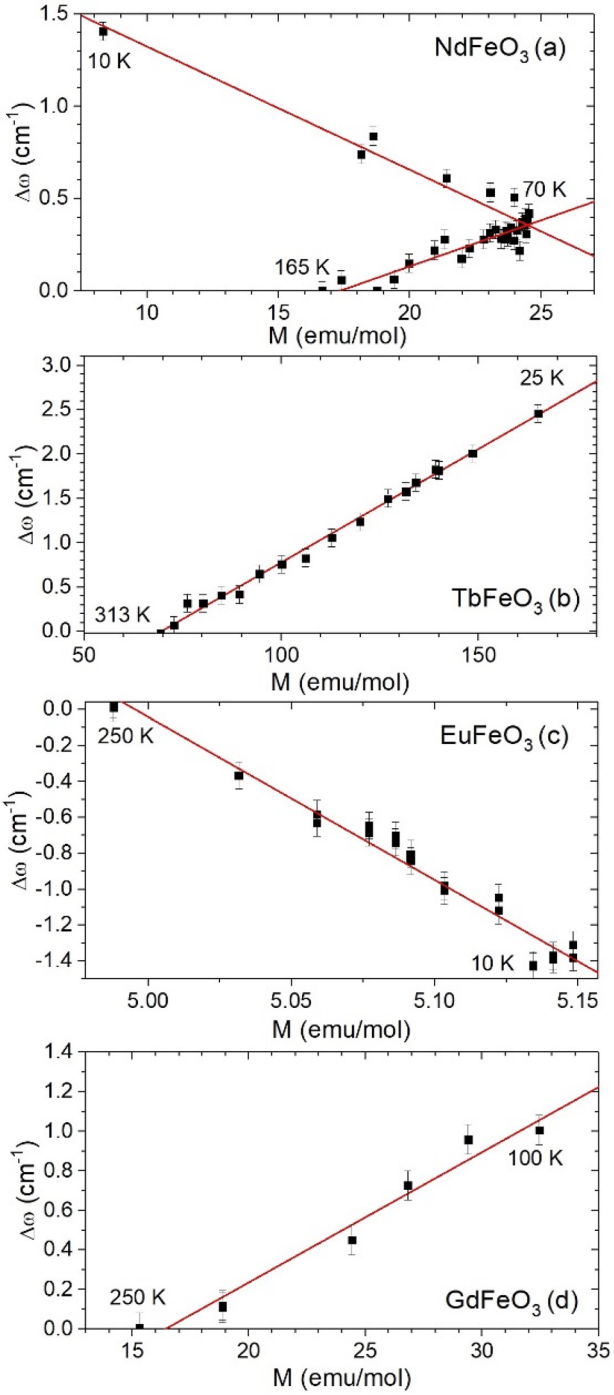

Figure 8. Anomalous contribution to the wavenumber of the $[010]_{pc}$ in-phase octahedra rotations of (**a**) $NdFeO_3$ (20–165 K), (**b**) $TbFeO_3$ (25–313 K), (**c**) $EuFeO_3$ (10–250 K), and (**d**) $GdFeO_3$ (100–250 K) as a function of the measured magnetization.

The relation between Δω and the measured magnetization is shown in Fig. 8a–d (see Fig. S4 of Supplemental Material for a wider temperature range). For $NdFeO_3$ (Fig. 8a), two linear regimes are found: one below 165 K encompassing the spin reorientation process, and another below 70 K, during the Nd^{3+} spins ordering process. Apparently, the different slopes of the linear relations result from the different mechanisms involved in each process.

For $TbFeO_3$, a unique linear dependence is observed, from 313 to 25 K. Below 25 K no linearity is observed, which could be associated with precursor effects of the spin-reorientation taking place at 20 K. In $EuFeO_3$ and $GdFeO_3$ (Fig. 8c,d), the unique linear dependence found below 250 K shows that these wavenumbers deviations origin from the magnetic changes, seen here via the spin–phonon coupling. In $GdFeO_3$ this linearity is lost below 100 K, where strong non-monotonous variations of the M(T) curve are observed. This quantitative analysis allows

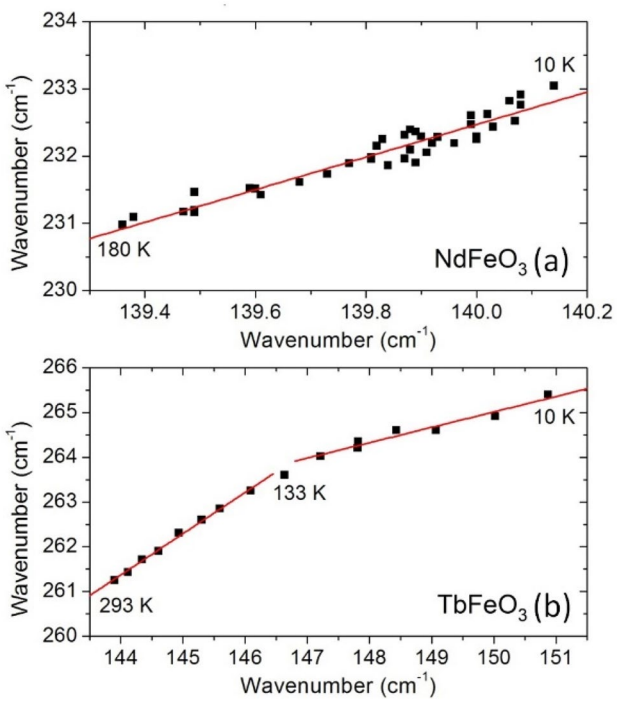

Figure 9. Wavenumber of the $[010]_{pc}$ in-phase octahedra rotation mode as a function of the wavenumber for the (**a**) Nd(*z*) and (**b**) Tb(*z*) out-of-phase oscillation modes, from 10 to 180 K and to 293 K, respectively.

us to state that the found magnetostructural effect results from a linear spin–phonon coupling that mediates the $[010]_{pc}$ in-phase octahedra rotational phonon and the magnetic structure.

To further evidence that the Nd(z)- and Tb(z)-oscillation modes are sensing the same phenomena of the $[010]_{pc}$ in-phase octahedra rotation mode, we have studied the correlation between their wavenumbers, shown in Fig. 9. We chose the R(z) instead of the R(x), because for the case of $TbFeO_3$ only the former shows a deviation similar to the FeO_6 rotation mode. The linear correlations between their wavenumbers found in the analyzed temperature ranges evidence for a coupling between them, with an unknown phenomenologically proportionality constant. For $TbFeO_3$, around 133 K, within the temperature interval where the slope of the linear temperature dependencies of both the $F(t)$ and M1 wavenumber curves changes the most, there is also a change of the found phenomenologically proportionality constant between these modes. This could not be observed in $GdFeO_3$ due to the absence of coupling between the Gd^{3+} motions and spins.

Conclusions

We have reported an experimental study of the magnetization, Raman-active spin excitations and lattice dynamics in $RFeO_3$ (R = Nd, Eu, Gd, and Tb) in the 10 to 850 K range. The main outcomes are summarized in the following.

Besides the known spin-reorientation of $NdFeO_3$, anomalies in the temperature dependence of magnetization and wavenumber of both the magnons and the FeO_6 rotation modes evidence for magnetic changes in $TbFeO_3$, $EuFeO_3$ and $GdFeO_3$, between 25 and 350 K, which are not associated with symmetry breaking nor magnetic phase transitions. The reinforcement of the ferromagnetic response of $TbFeO_3$ and $GdFeO_3$ is evidenced by both the increasing of magnetization as temperature decreases, and the anomalous temperature behavior of the ferromagnetic mode (magnon M1) at specific temperatures.

The sensitivity of the optical phonons to the Fe–Fe and *R*–Fe magnetic interactions was evidenced. The linear dependence on the magnetization of the anomalous contribution to the phonon wavenumber, just below the temperature where anomalies in M(T) are observed, distinctly bears the coupling between the $[010]_{pc}$ in-phase FeO_6 rotation mode and the spin structure, through a linear spin–phonon coupling. Thus, the second main outcome concerns the common magnetostructural coupling, evidenced by FeO_6 octahedra rotations. Like the FeO_6 rotational modes, the Raman-active *R*-oscillation modes are sensitive to the *R*–Fe magnetic interactions, provided a strong spin–phonon coupling mediated by spin–orbit coupling. In $NdFeO_3$ and $TbFeO_3$, wherein spin–orbit coupling of the *R*-cations exists, *R*-oscillations are coupled to the $[010]_{pc}$ in-phase octahedra rotational modes. The experimental results give strong evidence for the cross-talk between Fe^{3+} and Nd^{3+}/Tb^{3+} spin sublattice, denoting the third main outcome of this work. The largest variations of the magnon M1 and both studied Raman modes are the largest for $TbFeO_3$. Moreover, the smaller spin–phonon coupling strength found for the Nd-oscillations in $NdFeO_3$ suggests that the anisotropy of the Nd–Fe interaction plays a more important role on triggering the spin-reorientation at higher temperatures rather than its strength. Contrarily though, no deviation

of these two modes could be observed for $GdFeO_3$, demonstrating the key role played by the spin–orbit coupling to underlie the interplay between spins and the Gd-oscillation phonon.

Data availability

The datasets used and/or analyzed during the current study available from the corresponding author on reasonable request.

Received: 22 March 2022; Accepted: 20 May 2022
Published online: 11 June 2022

References

1. Gilleo, M. A. Magnetic properties of a gadolinium orthoferrite, $GdFeO_3$ crystal. *J. Chem. Phys.* **24**, 1239–1243 (1956).
2. Treves, D. Studies on orthoferrites at the Weizmann Institute of Science. *J. Appl. Phys.* **36**, 1033 (1965).
3. Bertaut, E. F., Chappert, J., Mareschal, J., Rebouillat, J. P. & Sivardière, J. Structures magnetiques de $TbFeO_3$. *Solid State Commun.* **5**, 293–298 (1967).
4. Eibschütz, M., Shtrikman, S. & Treves, D. Mössbauer studies of Fe_{57} in orthoferrites. *Phys. Rev.* **156**, 562–577 (1967).
5. White, R. L. Review of recent work on the magnetic and spectroscopic properties of the rare-earth orthoferrites. *J. Appl. Phys.* **40**, 1061 (1969).
6. Gordon, J. D., Gorodetsky, G. & Hornreich, R. M. Magnetization studies of $TbFeO_3$. *J. Magn. Magn. Mater.* **3**, 288–294 (1976).
7. Yuan, S. J. *et al.* Spin switching and magnetization reversal in single-crystal $NdFeO_3$. *Phys. Rev. B* **87**, 184405 (2013).
8. Zhao, Z. Y. *et al.* Ground state and magnetic phase transitions of orthoferrite $DyFeO_3$. *Phys. Rev. B* **89**, 224405 (2014).
9. Zhao, H. J., Bellaiche, L., Chen, X. M. & Íñiguez, J. Improper electric polarization in simple perovskite oxides with two magnetic sublattices. *Nat. Commun.* **8**, 14025 (2017).
10. Artyukhin, S. *et al.* Solitonic lattice and Yukawa forces in the rare-earth orthoferrite $TbFeO_3$. *Nat. Mater.* **11**, 694–699 (2012).
11. Tokunaga, Y., Iguchi, S., Arima, T. & Tokura, Y. Magnetic-field-induced ferroelectric state in $DyFeO_3$. *Phys. Rev. Lett.* **101**, 097205 (2008).
12. Tokunaga, Y. *et al.* Composite domain walls in a multiferroic perovskite ferrite. *Nat. Mater.* **8**, 558–562 (2009).
13. Bousquet, E. & Cano, A. Non-collinear magnetism in multiferroic perovskites. *J. Phys. Condens. Matter* **28**, 123001 (2016).
14. Bertaut, E. F. Configurations magnétiques. Méthode de fourier. *J. Phys. Chem. Solids* **21**, 256–279 (1961).
15. Tokunaga, Y., Taguchi, Y., Arima, T. H. & Tokura, Y. Electric-field-induced generation and reversal of ferromagnetic moment in ferrites. *Nat. Phys.* **8**, 838–844 (2012).
16. Senn, M. S. & Bristowe, N. C. A group-theoretical approach to enumerating magnetoelectric and multiferroic couplings in perovskites. *Acta Crystallogr. Sect. A Found. Adv.* **74**, 308–321 (2018).
17. Zhao, H. J., Íñiguez, J., Chen, X. M. & Bellaiche, L. Origin of the magnetization and compensation temperature in rare-earth orthoferrites and orthochromates. *Phys. Rev. B* **93**, 014417 (2016).
18. Moreira, J. A. *et al.* Coupling between phonons and magnetic excitations in orthorhombic $EuYMnO_3$. *Phys. Rev. B* **81**, 054447 (2010).
19. Weingart, C., Spaldin, N. & Bousquet, E. Noncollinear magnetism and single-ion anisotropy in multiferroic perovskites. *Phys. Rev. B Condens. Matter Mater. Phys.* **86**, 094413 (2012).
20. Park, B. G. *et al.* Magnetic properties of the orthoferrites $TbFeO_3$ and ErFeO 3. *J. Korean Phys. Soc.* **53**, 758–762 (2008).
21. Zhou, Z., Guo, L., Yang, H., Liu, Q. & Ye, F. Hydrothermal synthesis and magnetic properties of multiferroic rare-earth orthoferrites. *J. Alloys Compd.* **583**, 21–31 (2014).
22. Vilarinho, R. *et al.* Dzyaloshinskii Moriya nature of ferroelectric ordering in magnetoelectric $GdYMnO_3$ system. *Solid State Commun.* **208**, 34–40 (2015).
23. Ramesh Babu, P. *et al.* Investigation of magnetic property of $GdFeO_3$ single crystal grown in air by optical floating zone technique. *J. Alloys Compd.* **631**, 232–236 (2015).
24. Van Vleck, J. H. Magnetic case history of the Eu^{3+} ion. *J. Appl. Phys.* **39**, 365–372 (1968).
25. Mihalik, M. *et al.* Magnetic phase diagram of the TbMn1-xFexO_3 solid solution system. *Phys. B Condens. Matter* **506**, 163–167 (2017).
26. White, R. M., Nemanich, R. J. & Herring, C. Light scattering from magnetic excitations in orthoferrites. *Phys. Rev. B* **25**, 1822 (1982).
27. Venugopalan, S., Dutta, M., Ramdas, A. K. & Remeika, J. P. Magnetic and vibrational excitations in rare-earth orthoferrites: A Raman scattering study. *Phys. Rev. B* **31**, 1490 (1985).
28. Koshizuka, N. & Hayashi, K. Raman scattering from magnon excitations in $RFeO_3$. *J. Phys. Soc. Jpn.* **57**, 4418–4428 (1988).
29. White, R. M., Nemanichi, R. J. & Tsang, C. Raman scattering from magnons in rare earth orthoferrites. *J. Magn. Magn. Mater.* **15–18**, 773–774 (1980).
30. Jiang, J. *et al.* Dynamical spin reorientation transition in $NdFeO_3$ single crystal observed with polarized terahertz time domain spectroscopy. *Appl. Phys. Lett.* **103**, 062403 (2013).
31. Song, G. *et al.* Spin reorientation transition process in single crystal $NdFeO_3$. *Solid State Commun.* **211**, 47–51 (2015).
32. Yamaguchi, K., Kurihara, T., Minami, Y., Nakajima, M. & Suemoto, T. Terahertz time-domain observation of spin reorientation in orthoferrite $ErFeO_3$ through magnetic free induction decay. *Phys. Rev. Lett.* **110**, 137204 (2013).
33. Grishunin, K. *et al.* Terahertz magnon-polaritons in $TmFeO_3$. *ACS Photon.* **5**, 1375–1380 (2018).
34. Weber, M. C. *et al.* Raman spectroscopy of rare-earth orthoferrites $RFeO_3$ (R = La, Sm, Eu, Gd, Tb, Dy). *Phys. Rev. B* **94**, 214103 (2016).
35. Balkanski, M., Wallis, R. F. & Haro, E. Anharmonic effects in light scattering due to optical phonons in silicon. *Phys. Rev. B* **28**, 1928 (1983).
36. Ponosov, Y. S. & Novoselov, D. Y. Lattice and spin excitations of $YFeO_3$: A Raman and density functional theory study. *Phys. Rev. B* **102**, 054418 (2020).
37. Laverdière, J. *et al.* Spin–phonon coupling in orthorhombic $RMnO_3$ (R=Pr, Nd, Sm, Eu, Gd, Tb, Dy, Ho, Y): A Raman study. *Phys. Rev. B* **73**, 214301 (2006).
38. Bhadram, V. S., Rajeswaran, B., Sundaresan, A. & Narayana, C. Spin–phonon coupling in multiferroic $RCrO_3$ (R-Y, Lu, Gd, Eu, Sm): A Raman study. *Europhys. Lett.* **101**, 17008 (2013).
39. Kovaleva, N. N. *et al.* Anomalous multi-order Raman scattering in $LaMnO_3$: A signature of quantum lattice effects in a Jahn-Teller crystal. *J. Phys. Condens. Matter* **25**, 155602 (2013).
40. Weber, M. C. *et al.* Emerging spin–phonon coupling through cross-talk of two magnetic sublattices. *Nat. Commun.* **13**, 443 (2022).

Acknowledgements
We are deeply acknowledged to J. L. Ribeiro for the fruitful discussion regarding the interpretation of the magnetic data, and P. Bouvier suggestions on the analysis of some specific phonons. We acknowledge funding from NORTE-01-0145-FEDER-022096, UID/NAN/50024/2019 and PTDC/NAN-MAT/28538/2017 projects and R.V. to the grant from PTDC/NAN-MAT/0098/2020.

Author contributions
P.T. produced the samples. R.V. performed magnetization measurements. R.V., M.W. and A.M. performed Raman spectroscopy measurements. C.D. wrote an algorithm for Raman spectra analysis. R.V., M.W., M.G., J.K., A.A. and J.M. wrote the main manuscript text and R.V. prepared figures. All authors reviewed the manuscript.

Competing interests
The authors declare no competing interests.

Additional information
Supplementary Information The online version contains supplementary material available at https://doi.org/10.1038/s41598-022-13097-1.

Correspondence and requests for materials should be addressed to R.V.

Reprints and permissions information is available at www.nature.com/reprints.

Publisher's note Springer Nature remains neutral with regard to jurisdictional claims in published maps and institutional affiliations.